

Spectroscopic Study of the Symmetries and Deformation-Potential Constants of Singly Ionized Zinc in Germanium. Experiment*

Fernando Barra,[†] P. Fisher, and Sergio Rodriguez

Department of Physics, Purdue University, West Lafayette, Indiana 47907

(Received 18 December 1972)

This paper presents the experimental part of a piezospectroscopic study of the symmetries and deformation-potential constants of the energy states of singly ionized zinc in germanium. From the behavior of the excitation spectrum of this impurity under uniaxial compressions along the $\langle 111 \rangle$ and $\langle 100 \rangle$ directions, symmetry assignments have been made for the ground state and the excited states of the C and D lines, and it is found that $d' = -2.18 \pm 0.06$ eV, $d'_D = 0.15 \pm 0.03$ eV, $b' = -0.65 \pm 0.03$ eV, and $b'_D = 0.61 \pm 0.02$ eV, where these are deformation-potential constants for the ground state of the impurity and for the excited state of the D line. These conclusions were reached by making a detailed comparison of the experimental results with the theory and were corroborated by similar measurements with compression along a $\langle 110 \rangle$ axis.

I. INTRODUCTION

In a previous paper,¹ we discussed the theoretical basis for the interpretation of piezospectroscopic studies of the excitation spectra of single-hole acceptors in group-IV semiconductors. The present paper gives the results and interpretation of such an investigation for singly ionized zinc in germanium. Preliminary accounts of this work have been given elsewhere.^{2,3} The reader is referred to I for an introduction to the subject and for the appropriate references.

II. EXPERIMENTAL PROCEDURE

Ingots of germanium doped with zinc and antimony were prepared by first mixing pieces of pregrown zinc-doped germanium and antimony-doped germanium with pieces of pure germanium, and then growing single crystals using the Czochralski technique. No attempt has been made to determine the degree of compensation achieved, but each ingot used was p -type over its entire length. Of the three ingots that were made, samples cut from both ends of each ingot when cooled to near helium temperature exhibited an excitation spectrum that is thought to be characteristic of singly ionized zinc^{2,4} (see Sec. III). The spectrum was found to differ in quality at the two ends of an ingot and hence only that portion of an ingot that yielded the sharper set of excitation lines was used for sample preparation. Samples of different crystallographic orientation were cut from the "good" parts of the ingots, these being oriented either by x rays or by the optical method described by Hancock and Edelman.⁵ Optical samples were prepared by grinding the surfaces successively with No. 600, 1200, and 3200 carborundum and then etching to a "highly reflective" surface, a suitable wedge being included in the thickness of the sample to suppress channeled spectra. Single-beam double-pass Perkin-Elmer grating monochromators, Mod-

el 99-G, were used for the optical-absorption measurements; these were calibrated using the $15\text{-}\mu$ rotational-vibrational absorption spectrum of atmospheric carbon dioxide⁶ and the pure-rotational absorption spectrum of atmospheric water vapor.⁷ Unless otherwise specified all measurements were made with the use of a grating blazed for $20\ \mu$. A Reeder thermocouple⁸ with a diamond window was used as the detector. The samples were cooled to temperatures near that of liquid helium using a glass optical cryostat.⁹

Uniaxial compression was applied to the samples in two ways. The first employed a strain jig which utilized a differential-thermal-contraction technique similar to that described by Rose-Innes¹⁰ and Jones,¹¹ whereas the second method employed a quantitative-stress cryostat¹² in which a calibrated gas pressure was transmitted to a rod that pushed directly on the sample. In several measurements with the strain jig, two different samples, of half the length of the normal specimens, were placed end to end in the same jig. These "half" samples had the same cross-sectional area and hence experienced the same stress. In order that the transmission of each half sample could be studied independently, either the upper or the lower half of the entrance slit, depending on the sample, was masked. The spectra obtained under strain were studied using plane-polarized radiation produced by passing the infrared beam through a Perkin-Elmer wire-grid polarizer¹³ with either a silver chloride or a polyethylene substrate.

III. EXPERIMENTAL RESULTS AND DISCUSSION

A. Zero-Stress Spectrum

In Fig. 1 is shown a typical absorption spectrum obtained from a sample prepared in the manner described in Sec. II. A scan of the range $55.5\text{--}83.5$ meV has not revealed any extrinsic excitations

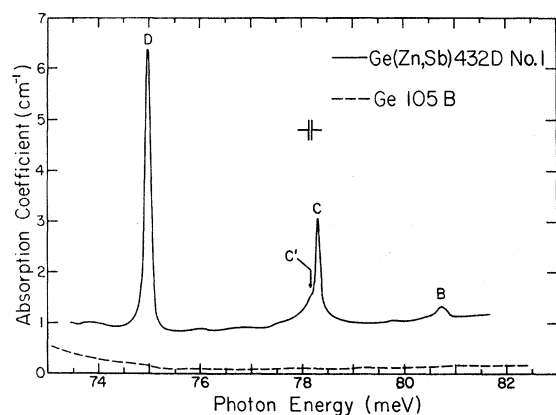


FIG. 1. The upper curve is the excitation spectrum of singly ionized zinc in germanium. Grating used was blazed for 12μ with 75 grooves per mm. The lower curve shows the absorption of pure germanium. Liquid helium used as coolant.

other than those shown. Also plotted in Fig. 1 is the absorption characteristic of essentially pure germanium, illustrating the level of lattice absorption in this spectral region. The positions of the lines *B*, *C*, and *D* are given in Table I. In each case the values given are an average of the results of a number of measurements. An estimate of the energy of the shoulder designated by *C'* is also included in the table. The energies given for the *C* and *D* lines are essentially the same as those obtained previously,^{2,4} but disagree with those reported by Sidorov *et al.*¹⁴ The energy spacings *B* to *C*, *C* to *C'*, and *C* to *D* are also given in Table I and compared with those of neutral zinc.¹¹ It should be noted that if the spacings *B* to *C'* and *C'* to *D* are compared with *B* to *C* and *C* to *D* of neutral zinc, then the ratios obtained are 4.20 ± 0.17 and 4.04 ± 0.21 , respectively.

Figure 2 gives more details of the lines *C* and *C'*. This figure was constructed by first subtracting the background absorption to give the full curve, then folding the high-energy side of the *C* line over onto its low-energy side (this gives the dashed curve), and finally subtracting the two curves to give the dotted curve. The asymmetric shape of the dotted curve is characteristic of that which is obtained when the above procedure is followed with other measurements of this spectrum. It suggests that *C'* may not be due to only one type of transition. An alternative explanation is that *C'* is very broad and also gives rise to the high-energy wing of the *C* line. In this case, the *C'* line could be due to a single transition, but it is not clear why it should be so broad.

The half-widths of the lines *C* and *D* in Fig. 1 are about 0.13 meV, which is essentially the same as the widths of the excitation lines of group-III¹⁵ and

TABLE I. Energies and energy spacings in meV of singly ionized zinc in germanium.

Line	Energy ^a (meV)	Spacing (meV)	Spacing relative to neutral zinc ^b
<i>B</i>	80.697 ± 0.011	<i>B-C</i> 2.371 ± 0.013	3.82 ± 0.15
<i>C</i>	78.326 ± 0.002	<i>C-C'</i> 0.136 ± 0.042	...
<i>C'</i>	78.19 ± 0.04	<i>C-D</i> 3.332 ± 0.007	4.38 ± 0.13
<i>D</i>	74.944 ± 0.005		

^aExcept in the case of *C'*, six or more measurements have been averaged for these values.

^bIn this column is shown the ratio of the energy spacings of the lines of singly ionized zinc to the corresponding spacings of the lines of neutral zinc in germanium. The excitation lines of the latter impurity have the energies 31.48 ± 0.01 , 30.86 ± 0.01 , and 30.10 ± 0.01 meV, respectively, for the *B*, *C*, and *D* lines (see Ref. 11).

neutral-zinc^{11,16} acceptors in germanium; line *B* is about twice as broad. Samples cut from two other ingots have also been studied. All ingots were prepared in the same way but the latter two contained a higher concentration of Zn⁻. The excitation lines observed for samples cut from different parts of these ingots exhibited considerable variations in width. In some cases line *B* was not observed and *C* and *D* were very broad. We attribute this to a Stark effect resulting from the variation in concentration of ionized impurities in these highly compensated ingots. The absorption spectrum of one of these samples was also examined in the spectral region where the excitation spectrum of neutral zinc occurs.^{4,11,16,17} No such spectrum was observed, indicating that the compensation was effective. A broadening effect can also be produced if the impurity concentration becomes high enough to cause significant overlap of wave functions of different impurities. However, for Zn⁻, the wave functions are more localized than for neutral acceptors and hence concentration broadening should oc-

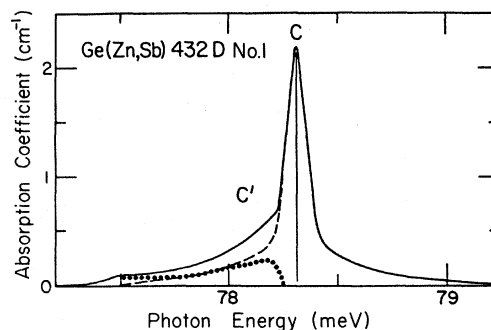


FIG. 2. *C* and *C'* excitation lines of singly ionized zinc in germanium. The full curve is that of Fig. 1 with the background absorption subtracted. The dashed curve is the result of folding the high-energy side of *C* over to the low-energy side. The dotted curve is the result of subtracting the dashed curve from the full curve.

cur at much larger concentrations than for neutral acceptors.

A comparison of the relative intensities of the lines *B*, *C*, and *D* of Fig. 1 with those of neutral zinc,^{4,11,15-17} neutral copper,^{4,17,18} neutral beryllium,¹⁹ and neutral mercury^{17,20,21} in germanium, reveals that qualitatively they are the same. This is part of the basis for the labeling. The fact that the energy spacings of the lines in Fig. 1 are nearly four times those of their counterparts for neutral zinc is strong evidence that the correlation made is valid. Further verification of this point will be obtained in Sec. IIIB where the symmetries of the energy states are elucidated by the piezospectroscopic studies of the spectrum.

The implication of the above is that a fairly accurate description of the excited *p*-like states of Zn^- in germanium can be obtained from the effective-mass theory for acceptors²² by simply altering the charge on the impurity ion from $-e$ to $-2e$, i. e., from a neutral heliumlike acceptor to an ionized heliumlike acceptor. The deviation of the ratio from four could be explained considering that, unlike ionized helium, the impurity ion possesses a large number of core electrons whose effectiveness is shielding the nucleus may vary from one excited state to another. Since we are dealing with a hole bound to a negative ion, this would imply that the maximum value this factor can have is four, corresponding to complete screening of the impurity nucleus by the core and valence electrons. This assumes that perfect screening occurs for the excited one-hole states of neutral zinc, a not unreasonable assumption since these states are much less tightly bound than the Zn^- states. This assumption is also borne out by experiment, since the energy spacings of corresponding excitation lines of all the neutral acceptors in germanium that have been studied so far are practically identical (see Table VI of Ref. 23) even though the nuclear charges vary widely and the number of bound holes ranges from one to three. However, this effect could explain only the *B* to *C* ratio (< 4) not the *C* to *D* ratio (> 4). A ratio in excess of 4 can be understood in the following manner. The deeper-lying states have wave functions that deviate from the effective-mass states in that the density of holes is largest along the tetrahedral directions where the valence-electron density is also highest. This can also be regarded as a deviation from the effective-mass potential expressed as a sum of multipole terms²⁴ appropriate to the symmetry T_d . This gives rise to a binding energy higher than expected from the effective-mass approximation for the low-lying states.

If the above identification of the excitation lines is correct, then we can calculate approximately the spacing of the excited states for the *C* line of the

neutral acceptors. Comparison of the results of the effective-mass calculations²² with experiment^{15,25} suggests that the final state of the *C* line could be either a Γ_8 state or a Γ_7 state or a combination of these two; the calculated spacing of these states is 0.10 meV. From the spacing of *C* and *C'* in Table I, it is seen that a value of ~ 0.03 meV would be predicted for the *C* to *C'* spacing for neutral acceptors, thus making the *C'* line difficult to resolve.

In the above, it is assumed that the acceptor being studied in the present measurements is singly ionized zinc. Samples prepared in the way already described yield essentially the same spectrum; this is true for the present and previous^{4,14} measurements. Mass spectrographic analysis²⁶ of the present samples show that each contains about equal parts of zinc, antimony, silicon, and magnesium, and a somewhat smaller concentration of aluminum. The silicon and aluminum should not produce the observed spectrum; however, the effect of magnesium is not clear. This acts as a double donor in silicon,²⁷ in which it is presumably an interstitial. If it has the same role in germanium, then it will merely serve, along with the antimony, to compensate the zinc and will be doubly ionized since all the samples studied were *p* type. But if it is a substitutional impurity in germanium, and hence a double acceptor,²⁸ it could be this impurity that gives rise to the ionized-heliumlike-acceptor spectrum under study. However, much higher concentrations of zinc can be introduced into germanium using the Czochralski technique than is possible for magnesium²⁸ and hence it is difficult to understand the origin of the high magnesium concentration. With the above reservations in mind, we shall continue to attribute the spectrum of Fig. 1 to singly ionized zinc. In support of this, the following study should be mentioned. When the spectrum of Fig. 1 is examined at liquid-nitrogen temperature, the *D* line shifts in energy to ~ 75.9 meV and broadens markedly, the *C* line becoming a shoulder on the high-energy side of the *D* line.^{29,30} A preliminary investigation of the absorption due to uncompensated zinc-doped germanium at the same temperature and in the same spectral range revealed a broad feature with a peak very close to this energy.²⁹ The implication of this is that the spectrum of Fig. 1 is due to singly ionized zinc.

B. Effect of Uniaxial Stress

1. Applied Force Along $\langle 111 \rangle$ Axis

The behavior of the spectrum of Fig. 1 under uniaxial compression along $\langle 111 \rangle$ axis is illustrated in Figs. 3 and 4. The compressive force \vec{F} has been applied with the strain jig in both cases. The magnitudes of the splittings of the components of the *D* line provide gauges of the stress achieved in each case. It is clear that \vec{F} is larger for the spec-

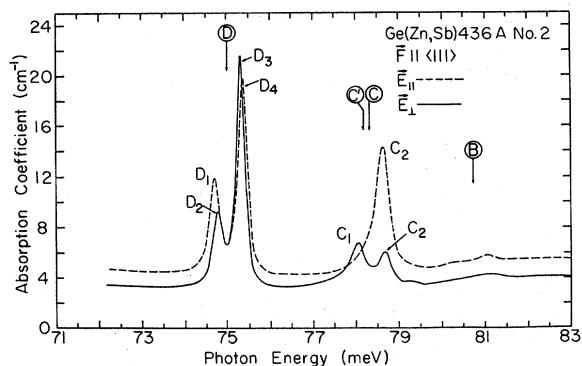


FIG. 3. Stress-induced spectrum of singly ionized zinc in germanium for a compressive force \vec{F} along a $\langle 111 \rangle$ axis using the strain jig. The vertical arrows and circled letters indicate the zero-stress positions. Liquid helium used as coolant.

trum of Fig. 4 than for that of Fig. 3. This is also borne out by the differences in the intensities of the lower-energy components of both the C and D lines for both figures; the absorption spectra in the two cases were obtained under experimental conditions that should have produced the same sample temperature. In these spectra, and those that follow, the results obtained with the electric vector \vec{E} parallel to \vec{F} ($E_{||}$) are plotted with a dashed line while those for $\vec{E} \perp \vec{F}$ (E_{\perp}) are represented by full curves.

In the interpretation of the data to be discussed later in this section, the splitting of the ground state Δ'_{111} is gauged by taking the mean of the difference in energy of the components D_1 and D_3 and D_2 and D_4 . In Fig. 5 are presented the results of a number of measurements in which the energies of the components of the various lines are plotted as a function of Δ'_{111} . The straight lines represent the results of least-squares fits to the data. In the

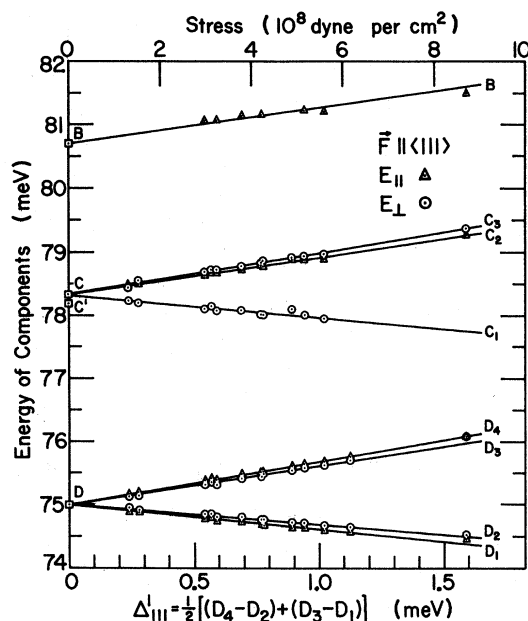


FIG. 5. Dependence of the energy of the stress-induced components of the spectrum of singly ionized zinc in germanium on the splitting of the ground state Δ'_{111} . The straight lines are least-squares fits to the data. The calibration of Δ'_{111} in terms of stress is discussed in the text.

case of B and D components, where no ambiguity exists regarding their origins, a number of zero-stress values have been included in the fits. However, for the C components no zero-stress values have been used and it can be seen that all three components, C_1 , C_2 , and C_3 , appear to stem from C and not C' . In Figs. 3 and 4, and other similar measurements, there is a clear suggestion of a broad low-energy tail to C_2 , which is presumably due to C' .

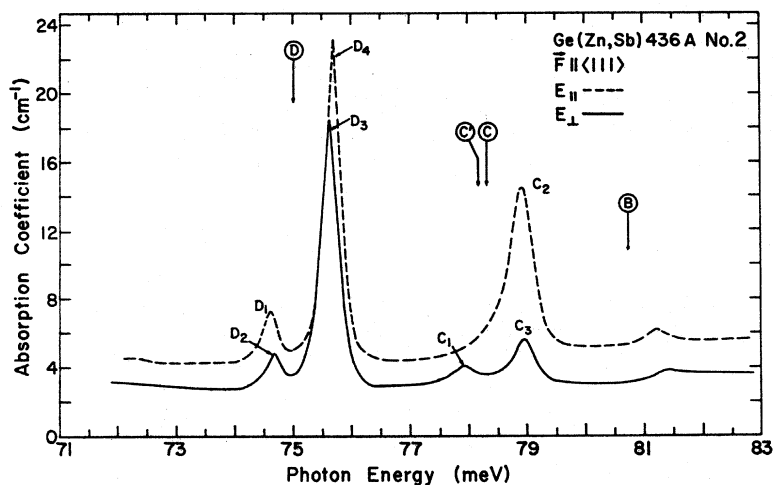


FIG. 4. Same as Fig. 3 but at a larger stress.

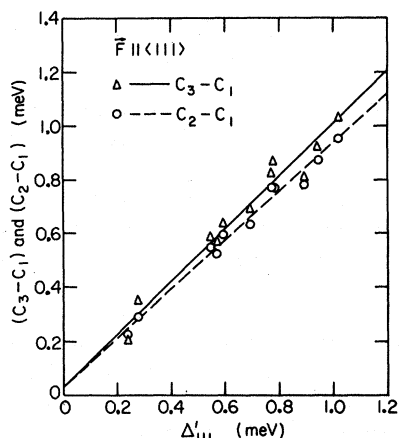


FIG. 6. Dependence of the energy spacings of the pairs of components C_1 and C_2 and C_1 and C_3 on Δ'_{111} for $\bar{F} \parallel \langle 111 \rangle$. The straight lines are least-squares fits to the data.

A plot of the differences in energies of the pairs C_1 and C_2 and C_1 and C_3 as a function of Δ'_{111} is shown in Fig. 6. The straight lines represent the outcome of least-squares fits to these data, and suggest that C_1 and C_3 have a common final state.

The quantitative dependence of Δ'_{111} on stress is given in Fig. 7, where the stress is proportional to the pressure of the gas used with the stress cryostat.¹² Both methods for applying compressions were used since in the case of the strain jig, quantitative values of stress were not obtained, while for the present use of the stress cryostat completely reliable intensity measurements were not made. The straight line in Fig. 7 represents a least-squares fit to the data, and has the slope 0.04582 ± 0.00062 meV/(lb/in.²). From this result, the sample area (8.486 ± 0.052 mm²), and the calibration of the stress cryostat (4.788 ± 0.048 lbwt/

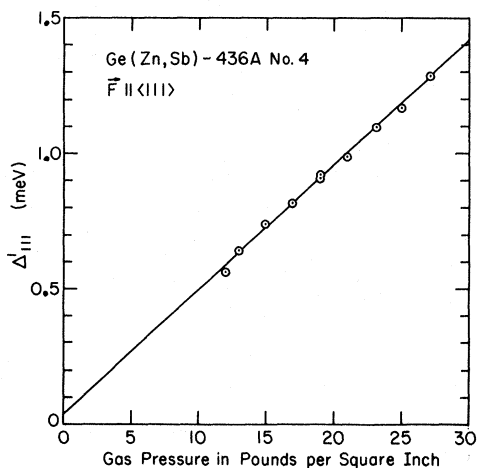


FIG. 7. Dependence of Δ'_{111} on gas pressure of the pressure head of the stress cryostat (see Ref. 12).

(lb/in.²),³¹ it is estimated that

$$|\Delta'_{111}| = (1.826 \pm 0.055) \times 10^{-9} |S|, \quad (1)$$

where Δ'_{111} is in meV if S , the stress, is in dyn/cm². It is this result that has been used to determine the upper scale in Fig. 5. Also it is found that

$$|\Delta_{111}^D| = (0.07 \pm 0.01) |\Delta'_{111}|. \quad (2)$$

If we assume that the D line is due to a $\Gamma_8 \rightarrow \Gamma_8$ transition,^{15,25} then we can interpret the present data using the results of I. Under a uniaxial force, a Γ_8 state splits into two twofold degenerate states. It is clear from the decrease in the intensities of components D_1 and D_2 relative to those of D_3 and D_4 as the stress is increased that D_1 and D_2 arise from the upper of the two states into which the Γ_8 ground state splits, while D_3 and D_4 originate from the lower of these. The number of components observed and their polarizations are consistent with the selection rules of, for example, Fig. 1 of I. Since three components are allowed for E_1 , the implication is that one of these is very weak, which in turn implies that u_D is fairly small (see either Table XIV of I or Fig. 2 of I). Before we can proceed further,

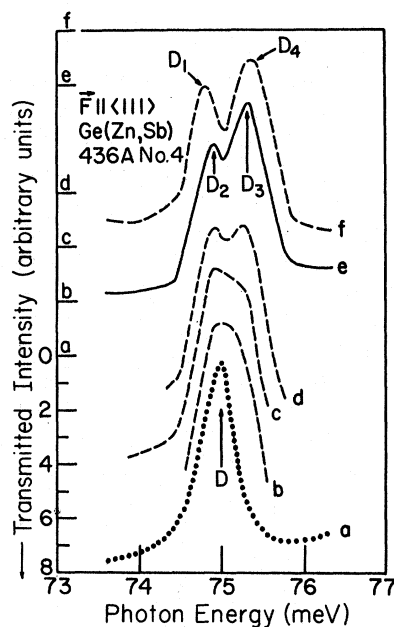


FIG. 8. Effect of small stresses on the D line of singly ionized zinc in germanium. The curves have been taken directly from the recorded signal transmitted by the sample. The stress is increasing, in alphabetical order, curve a being for zero stress. All curves are for E_{II} except curve e which was taken with E_1 at the same stress as curve f . The lettered graduations on the left ordinate designate the zero level of transmitted signal for the corresponding curve. Liquid helium used as coolant. Measurements obtained using the stress cryostat. For curves e and f , $|S| \approx 2.7 \times 10^8$ dyn/cm².

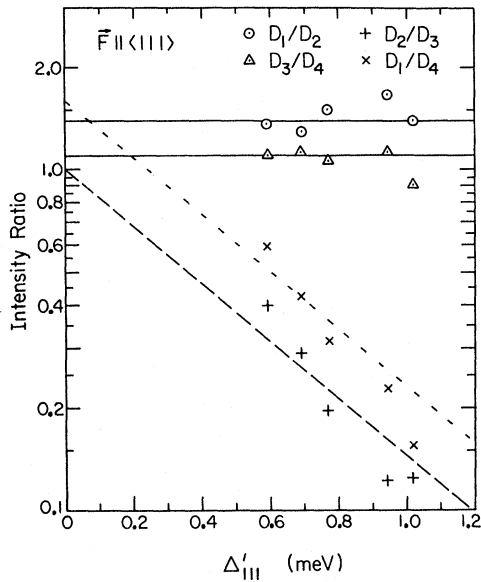


FIG. 9. Dependence of the ratios of the intensities of the D components for $\bar{F} \parallel \langle 111 \rangle$ on Δ'_{111} . The dashed lines have been drawn for a value of $u_D = 0.23$ (see text) and a sample temperature T of 6°K and are not fitted to the data. The full lines are the means of the four best data points in each case.

we must establish the origins of D_1 and D_4 . The data of Figs. 3 and 4 show D_1 to be stronger than D_4 . These, however, are not sufficient to establish the relative intensities of these two components since depopulation of the upper ground substate must be taken into account. It is possible to correct for this if the temperature of the sample is known, otherwise the ratio of the intensities of D_1 and D_4 as a function of Δ'_{111} could be plotted and extrapolated to zero strain. However, this latter procedure will not be particularly accurate if the sample temperature should change from one stress to another. The results given in Fig. 8 show that for equal population of the ground-state sublevels, D_1 is more intense than D_4 . In this figure, the behavior of the D line is shown as S is increased from 0 to $\sim 2.7 \times 10^8$ dyn/cm², the stress being zero for curve a and becoming progressively larger from a to f , except that e and f are for the same stress but different polarizations. Clearly in curve c , although D_1 and D_4 are not resolved, D_1 is larger than D_4 . For curve d they are of about equal intensity while for f , D_1 is less intense than D_4 . Curve e is presented in order to show that for the same conditions the ratio of the intensities of D_2 and D_3 is less than that of D_1 and D_4 , from which we infer that for equal population, D_2 and D_3 could be of equal intensity, as required by symmetry.¹

From the above information, we conclude that the

components D_1 , D_2 , D_3 , and D_4 correspond to the transitions $\Gamma_{5+6} \rightarrow \Gamma_{5+6}$, $\Gamma_{5+6} \rightarrow \Gamma_4$, $\Gamma_4 \rightarrow \Gamma_{5+6}$, and $\Gamma_4 \rightarrow \Gamma_4$, respectively. The ratio of the intensities of D_1 to D_2 or D_3 to D_4 can be used to determine u_D since these ratios do not involve depopulation effects.

The results of our most reliable intensity measurements are shown in Fig. 9; the intensity of each component has been estimated by measuring its area. If, for D_1/D_2 and D_3/D_4 , where the fractions denote ratios of intensities, we neglect the two points that are in poor agreement with the others, the means of the two ratios are, respectively, 1.39 ± 0.06 and 1.10 ± 0.02 , where the errors given represent the mean absolute deviations or average errors. From the expressions for the intensities, we obtain $u_D = 0.23 \pm 0.03$ from D_1/D_2 and $u_D = 0.17 \pm 0.03$ from D_3/D_4 . However, in the latter case, we should assume that the area associated with D_3 also includes D_4^1 , the third but weak component for E_1 . If we equate $(D_3^1 + D_4^1)/D_4^1$ to 1.10 ± 0.02 , we obtain $u_D \approx 0.06 \pm 0.01$. It should be pointed out that both D_3^1 and D_4^1 are intense components and for the sample thickness and impurity concentration used, the transmission at their peaks was only a few percent; hence some error is expected from this. In one measurement the components were broader than in the others, presumably because the stress was somewhat inhomogeneous. For this case, the peak heights of the lines were smaller and hence should be more reliable than for the other measurements; the ratio of the intensity of D_3 to that of D_4 for this observation was 1.12, which leads to a value of u_D of either 0.19 or 0.07, depending upon whether D_4^1 is included or not.

The ratio of the intensity of D_2 to that of D_3 should be independent of the value of u_D but vary as $e^{-\Delta'_{111}/kT}$. The long-dashed line in Fig. 9 is drawn for $T = 6^\circ\text{K}$ and has the intercept $D_2/D_3 = 1$. It is not an unreasonable fit to the data points for D_2/D_3 , particularly as the temperature of the sample may be somewhat different from one measurement to another. However, a value of $T = 6^\circ\text{K}$ is somewhat too small. From past experience,³² a value of $T \sim 10^\circ\text{K}$ would be more acceptable.

The fourth ratio plotted in Fig. 9 is that of D_1 to D_4 . This ratio is predicted¹ to be $[(1 + u_D)/(1 - u_D)] \times e^{-\Delta'_{111}/kT}$. The short-dashed line in Fig. 9 is drawn for $u_D = 0.23$ and $T = 6^\circ\text{K}$. This is also a reasonable fit to the data points for D_1/D_4 . It might also be noted that the results depicted in curve d of Fig. 8 are also consistent with this. If the value of $u_D = 0.06$ discussed above is used, then no fit at all is obtained.

From the orderings and splittings given above for the sublevels of the ground state and the excited state of the D line and Eq. (23) of I, the deformation-potential constants can be determined for these

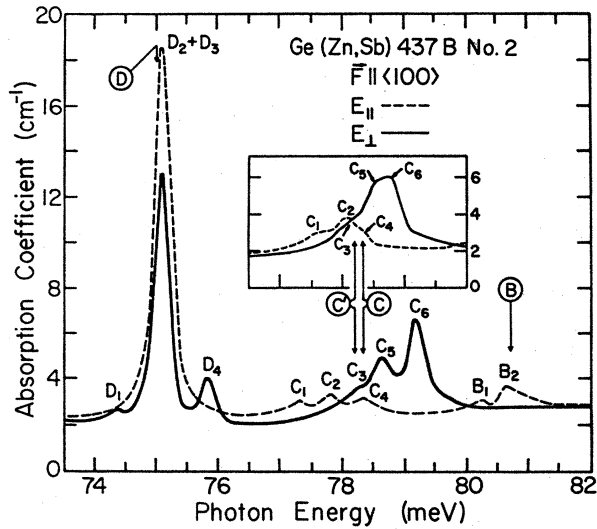


FIG. 10. Excitation spectrum of singly ionized zinc in germanium for $\vec{F} \parallel \langle 100 \rangle$. Liquid helium used as coolant. The inset shows the spectrum for the C line at a stress lower than that of the main figure. The strain jig was used in both cases.

two states. The values obtained are given in Table II. In addition, the shift in the center of gravity of the D components is found to be $(0.150 \pm 0.006) |\Delta'_{111}|$. From the stress dependence of Δ'_{111} , Eq. (1), a value has been obtained for the difference in the hydrostatic deformation-potential constant of the ground state (a') and that of the excited state of the D line (a'_D). This value is also given in Table II.

The simplest interpretation of the C line is that it is due to a transition to a Γ_8 or Γ_7 final state. In this case, one component is predicted for E_{\parallel} and two for E_{\perp} , which is in agreement with experiment if it is assumed that the energies of C_2 and C_3 coincide (see Fig. 6). The intensity ratios of C_1 , C_2 , and C_3 would need to be 3:4:1, which is not contradicted by the experiment (see Figs. 3 and 4). This interpretation is consistent with that given for

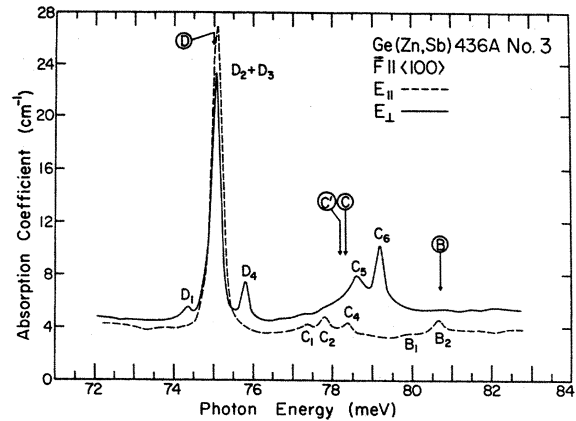


FIG. 11. Same as Fig. 10 but with about twice the resolution.

the Zeeman effect³⁵ on the C line of boron in germanium but is not compatible with the results obtained for $\vec{F} \parallel \langle 100 \rangle$ to be discussed below. From the data and Table XIV of I, we can rule out the possibility that the C line has a Γ_8 final state, the next simplest interpretation.

2. Applied Force Along $\langle 100 \rangle$ Axis

The behavior of the spectrum of Fig. 1 for a compressive force along a $\langle 100 \rangle$ direction is shown in Figs. 10–12. The results were obtained with the use of the strain jig. The inset of Fig. 10 shows the behavior of the C' and C lines at a strain smaller than that of the main figure. The spectrum given in Fig. 11 is for a strain close to that of Fig. 10. This result has been included in order to illustrate how the spectrum appears under the best resolution obtained with a very homogeneous stress. The resolution of Fig. 11 is about twice that of Figs. 10 and 12. However, the values of the absorption coefficients may not be as reliable as those of Fig. 10 since the absorption backgrounds for E_{\parallel} and E_{\perp} do not coincide in Fig. 11, whereas

TABLE II. Deformation-potential constants for energy states of singly ionized zinc in germanium. Units are eV; the symbols used to designate the deformation-potential constants are those of Refs. 25 and 33. The values of s_{11} , s_{12} , and s_{44} used have been obtained from the data of Ref. 34 for $T=10^\circ\text{K}$. The values so obtained are $s_{11}=9.585 \times 10^{-13} \text{ cm}^2/\text{dyn}$, $s_{12}=-2.6092 \times 10^{-13} \text{ cm}^2/\text{dyn}$, and $s_{44}=14.542 \times 10^{-13} \text{ cm}^2/\text{dyn}$. In calculating the deformation-potential constants, we have assumed the errors in the above quantities to be negligible compared to those arising from other sources. The present experiments do not enable one to determine the sign of b' . The sign we have chosen is the same as that of the corresponding parameter of the valence band as given in Ref. 37 (see text).

Orientation of \vec{F}	a'	b'	a'_D	b'_D	$a' - a'_D$
$\langle 111 \rangle$	$-(2.18 \pm 0.06)$...	0.15 ± 0.03	...	0.63 ± 0.05
$\langle 100 \rangle^a$...	$-(0.65 \pm 0.03)$...	0.61 ± 0.02	0.40 ± 0.05
$\langle 110 \rangle$	0.58 ± 0.05

^aIt should be noted that the errors specified for this case do not take into account the possibility that a systematic error may exist as a consequence of the method described in the text to find the stress dependence of D_3 .

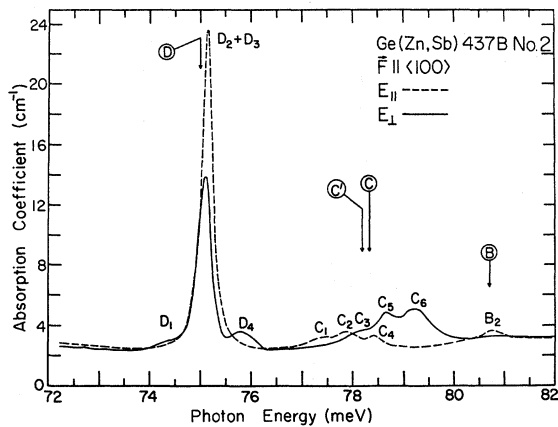


FIG. 12. Same as Fig. 10 but for a somewhat inhomogeneous stress.

they do in Figs. 10 and 12 and for all other measurements made with this direction of \vec{F} . The data in Fig. 12 show broadening of those components that are well displaced from the zero-stress positions; this is attributed to inhomogeneity in the stress. It is seen that the peak position of the very weak D_1 component becomes quite uncertain for inhomogeneous stresses. Also, it is found from other measurements that as the stress is increased, D_1 decreases, presumably because of increasing depopulation of the upper ground-state sublevel with stress.

The selection rules for $\vec{F} \parallel \langle 100 \rangle$ have been given in I. In the case of a $\Gamma_8 \rightarrow \Gamma_8$ transition, two components should be obtained for $E_{||}$ and four for E_{\perp} .

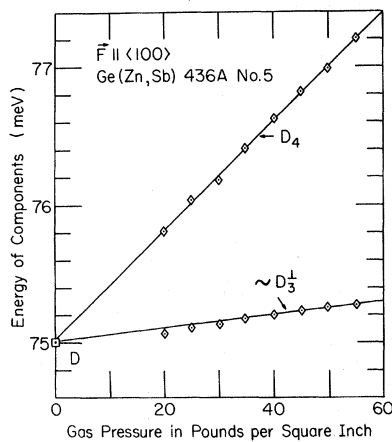


FIG. 13. Stress dependence of the energy of D_3 and D_4 for E_{\perp} with $\vec{F} \parallel \langle 100 \rangle$. The calibration of the pressure head used with the stress cryostat (see Ref. 12) was 4.788 lb wt/(lb/in.²) (see text). The straight line fitted to D_4 does not include any zero-stress values of D . The straight line designated by $\sim D_3^{1/2}$ is the fit to the energies of $D_2 + D_3$ at the four highest stresses.

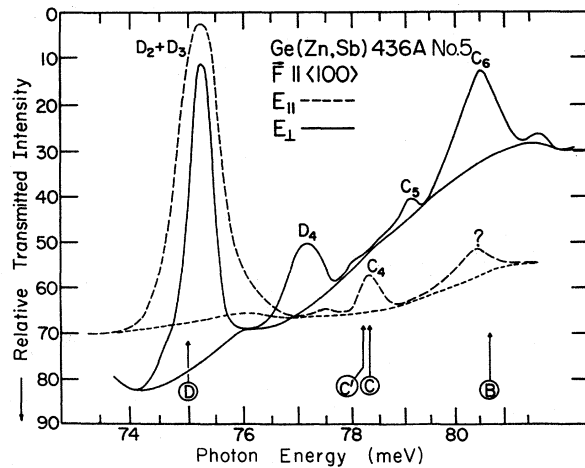


FIG. 14. Spectrum obtained with the stress cryostat corresponding to the data in Fig. 13 for a gas pressure of 55 lb/in.², which corresponds to a stress of $\sim 1.3 \times 10^9$ dyn/cm². The curves have been taken directly from the recorded signal transmitted by the sample. The smoothly varying backgrounds shown represent, approximately, the energy dependence of the intensity of the reference beam. Note that the abscissa is not linear in energy but is almost linear in wavelength.

If $\Delta'_{100} \approx \Delta^D_{100}$, then the observations conform to the predictions, since for both polarizations two components will be essentially superimposed and will lie close to the position of the zero-stress line. For the value of $u_D \approx 0.23$ deduced above, the two transitions $\Gamma_6 \rightarrow \Gamma_6$ and $\Gamma_7 \rightarrow \Gamma_7$ for E_{\perp} (see Table XV and Fig. 3 of I) will be weak compared to the composite line resulting from the superposition of the transitions $\Gamma_6 \rightarrow \Gamma_7$ and $\Gamma_7 \rightarrow \Gamma_6$ in either polarization. Hence, the strong component observed for each polarization and labeled $D_2 + D_3$ in Figs. 10–12 is interpreted to consist of these latter two transitions, and the relative ordering of the sublevels of the ground and excited states is assumed to be that of Fig. 1(b) of I. Since D_2 is not resolved from D_3 , an unambiguous determination of Δ'_{100} and Δ^D_{100} is difficult to obtain. The way we have proceeded is discussed below and involves combining the results obtained with the strain jig and the data taken using the quantitative-stress cryostat.

In Fig. 13 are shown the data obtained for the D components for E_{\perp} using the stress cryostat. In this measurement, D_1 was not well defined even at small stresses because of some inhomogeneity in the strain. The extent of this inhomogeneity may be understood in a qualitative way from the shape of the D_4 component in the spectrum of Fig. 14. These data were obtained with the stress cryostat at a measured gas pressure of 55 lb/in.². The energy dependence of the intensity of the incident radiation is represented by the relatively smoothly varying background curves for the two polarizations.

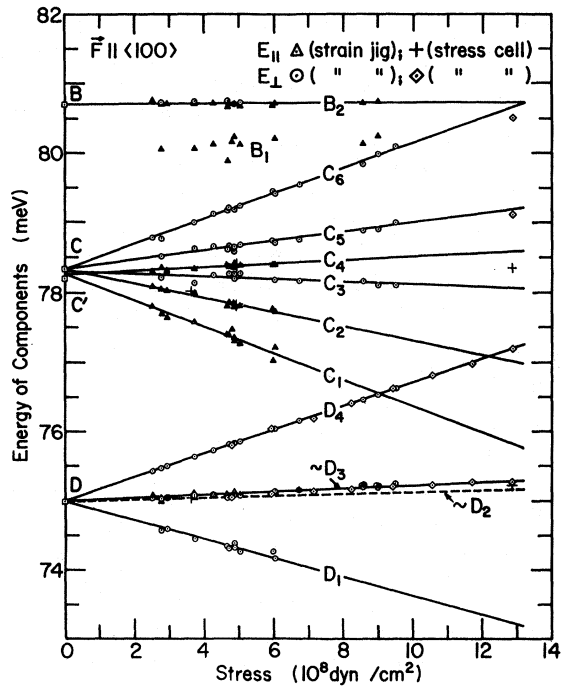


FIG. 15. Stress dependence of the components of the excitation lines of singly ionized zinc in germanium. The strain-jig and stress-cryostat measurements have been combined in this figure (see text).

A least-squares fit has been made to the data for D_4 excluding the zero-stress values for the D line. This gives the corresponding straight line shown in Fig. 13. It was necessary to exclude the zero-stress data in order to preserve the slope of the straight line since it is known that the pressure head used in the apparatus¹² introduces a small systematic error into the readings. From the slope of this line and the cross-sectional area of the sample, the stress dependence of the energy of D_4 has been found. With this result it is possible to calibrate each of the measurements obtained with the strain jig since D_4 is a well-defined component. The combined results are shown in Fig. 15. The data for D_4 obtained with the strain jig are also included in this plot but lie, of course, exactly on the straight line labeled D_4 .

If it is assumed that for gas pressures equal to and greater than 40 lb/in.² in Fig. 13, the contribution of D_2^1 to $D_2^1 + D_3^1$ is negligible, then a straight line fitted to the four points at these highest stresses should represent the stress behavior of D_3^1 . This straight line is designated by $\sim D_3^1$ in Fig. 13. The fit is consistent with the presence of a lower-energy component (D_2^1) which arises from the upper-ground-state sublevel and decreases at high stresses as depopulation effects become pronounced. A similar fit is shown in Fig. 15, where it is labeled by $\sim D_3$. In this fit, a correction to the systematic error in

the pressure head has been obtained from the fit to D_4 , and then the four high-stress points of Fig. 13 as well as the zero-stress values of D fitted to a straight line.

All the straight lines in Fig. 15 are the results of least-squares fits to the data. It should be pointed out that all such fits were made using the conventional forms of the least-squares-fit equations. In each case a fit was made of energy vs S and S vs energy and the average of the two fits taken, since the conventional equations assume no error in one of the variables.³⁶ The error obtained in each case was taken to be the larger of either the most probable error as given by the fit or half the difference between the two values obtained when the above fits were made.

From the fits to the D components, it is deduced that

$$|\Delta'_{100}| = (1.585 \pm 0.058) \times 10^{-9} |S| \quad (3)$$

and

$$|\Delta^D_{100}| = (1.492 \pm 0.040) \times 10^{-9} |S|, \quad (4)$$

where the units are the same as those of Eq. (1). The errors shown are due to the error in the sample area, the pressure head calibration, and the least-squares fits. From Eqs. (3) and (4), and Eq. (25) of I, the deformation-potential constants b' and b'_D have been determined; these are given in Table II. It should be noted that the present experiment only gives the relative signs of b' and b'_D . In Fig. 1(b) of I, the ordering of the stress-induced sublevels of the two Γ_8 states could be inverted simultaneously and still give agreement with experiment. For the effective-mass-like group-III impurities, it is predicted³³ that the signs of b' and d' are the same as their counterparts for the valence band³⁷; this is thought to be borne out by experiment.²⁵ Even though the ground state of Zn^- in germanium is far from being effective-mass-like, the sign of d' is the same as that of the group-III acceptors in germanium.²⁵ Hence we have chosen the sign of b' also to be the same as that of an effective-mass-like defect. For the present orientation, the difference between the hydrostatic shifts of the ground state and the excited state of the D line has also been determined; this value is included in Table II. It should be emphasized that the errors specified for the deformation-potential constants in this table for $\vec{F} \parallel \langle 100 \rangle$ do not take into account the possibility that a systematic error may exist as a consequence of the method used to find the stress dependence of D_3 .

From the stress dependence of the energies of the components D_1 , $\sim D_3$, and D_4 , an estimate has been made of the behavior of the unresolved D_2 component. This is designated by the dashed line labeled $\sim D_2$ in Fig. 15. There is some experimen-

tal evidence for D_2 . It is found that $D_2 + D_3$ for both directions of polarization is asymmetric, being broader on the low-energy side.

From the measured relative intensities of the strong components $D_2^+ + D_3^+$ and $D_2'' + D_3''$, and those predicted by Table XV of I, it is found that $v_D \approx \frac{1}{4}$. A value of $u_D = 0.23$ was used in making this estimate. The intensities of D_1 and D_4 are compatible with this result. In determining v_D , the temperature T of the sample is required, since the expressions in Table XV of I must be suitably scaled to take into account the populations of the two ground-state sublevels at a given value of Δ'_{100} . The ratio of the intensity of D_1 to that of D_4 should give an experimental estimate of the Boltzmann factor, $e^{-\Delta'_{100}/kT}$, at each stress. However, since both D_1 and D_4 are weak components, the value of $e^{-\Delta'_{100}/kT}$ determined in this way will not be very reliable. In fact, estimates of T obtained from this factor ranged from ~ 7 to ~ 15 °K. A realistic value of T for the present measurements is ~ 10 °K. This is the value which was used in the determination of the above value of v_D .³⁸ For $v_D = 0.25$, $u_D = 0.23$, and $T = 10$ °K, it is estimated that for the lowest stress used to find the stress dependence of D_3^+ , $\Delta'_{100} \approx 1.5$

meV and that the ratio of the intensity of D_2^+ to that of D_3^+ is $\sim \frac{1}{3}$, which justifies the assumption that at and above these stresses the position of D_3^+ is essentially given by that of $D_2^+ + D_3^+$. Another way to have determined the behavior of D_3 would have been to use $D_2'' + D_3''$, since, even at the lowest stresses, the ratio of the intensity of D_2'' to that of D_3'' is $\sim \frac{1}{3}$ (see, for example, Fig. 3 of I). However, for all the stresses used, no significant difference has been found between the positions of $D_2^+ + D_3^+$ and $D_2'' + D_3''$, thus further justifying the above procedure.

From the values of Δ'_{111} and Δ'_{100} given in Eqs. (1) and (4), it is found that

$$\left| \frac{\Delta'_{111}}{\Delta'_{100}} \right| = 1.22 \pm 0.05, \quad (5)$$

where the errors have been estimated from those of Eq. (1) and (4) but taking into account the fact that the 1% error in the calibration of the pressure head is common to both Δ'_{111} and Δ'_{100} . The result given in Eq. (5) has been verified by using two half samples (see Sec. II), one with a $\langle 111 \rangle$ orientation, the other with a $\langle 100 \rangle$ orientation. The results obtained in such a measurement are given in Fig. 16. The region designated by $\langle 100 \rangle$ in the $\vec{F} \parallel \langle 111 \rangle$ spectrum is due to some of the radiation also passing through the $\langle 100 \rangle$ sample. Similarly, in the $\vec{F} \parallel \langle 100 \rangle$ spectrum some of the radiation has also passed through the $\langle 111 \rangle$ sample. From the data of Fig. 16, a value of 1.21 ± 0.07 was obtained for $|\Delta'_{111}/\Delta'_{100}|$, in excellent agreement with the result in Eq. 5. Another measurement, similar to that of Fig. 16, but at a somewhat smaller stress, gave a value of 1.13 ± 0.13 .

Using the technique of half-samples, another determination of d' has been made by comparing the spectrum obtained with a half- $\langle 111 \rangle$ sample of Zn⁻ in germanium with that of a half- $\langle 100 \rangle$ sample of arsenic in silicon. The spectra obtained are given in Fig. 17. The notation used to label the stress-induced components of the arsenic spectrum is that of Ref. 39. For the conditions under which the two spectra in Fig. 17 were obtained,

$$\frac{\Delta E_{2p_{\pm}}}{\Delta'_{111}} = \frac{\Xi_u (s_{11} - s_{12})_{Si} \sqrt{3}}{d' s_{44}^{Ge}}, \quad (6)$$

where $\Delta E_{2p_{\pm}}$ is the splitting of the $2p_{\pm}$ component,¹² Ξ_u is the shear-deformation-potential constant of the bottom of the conduction band of silicon, and $(s_{11} - s_{12})_{Si}$ and s_{44}^{Ge} are elastic compliance constants for Si and Ge, respectively. From the known value¹² of Ξ_u and the data in Fig. 17, a value of 2.14 ± 0.17 eV was obtained for $|d'|$, in excellent agreement with the value given for this quantity in Table II.

In an attempt to determine which of C and C' is the parent line of a given component, no zero-stress values were used in making the fits in Fig.

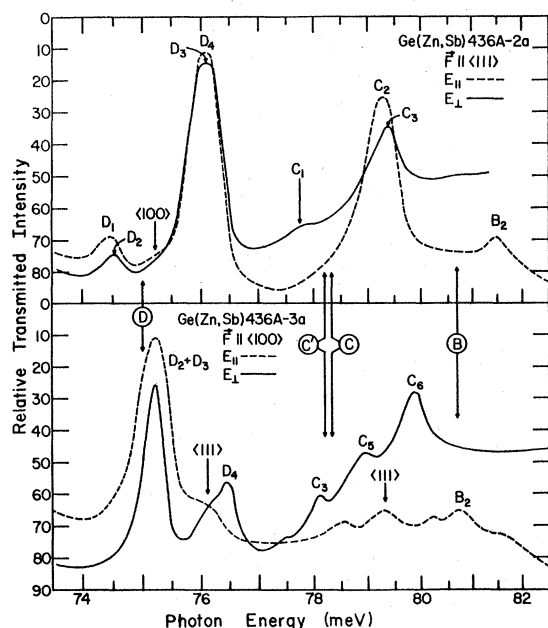


FIG. 16. Excitation spectra of singly ionized zinc in germanium from two half samples (see text), the upper spectrum being for $\vec{F} \parallel \langle 111 \rangle$ and the lower for $\vec{F} \parallel \langle 100 \rangle$. The regions designated by either $\langle 100 \rangle$ or $\langle 111 \rangle$ are a consequence of leakage of radiation through the sample whose transmission is not being studied. The spectra have been taken directly from the recorded signals transmitted by the samples. Liquid helium used as coolant. Note that the abscissa is not linear in energy but is almost linear in wavelength.

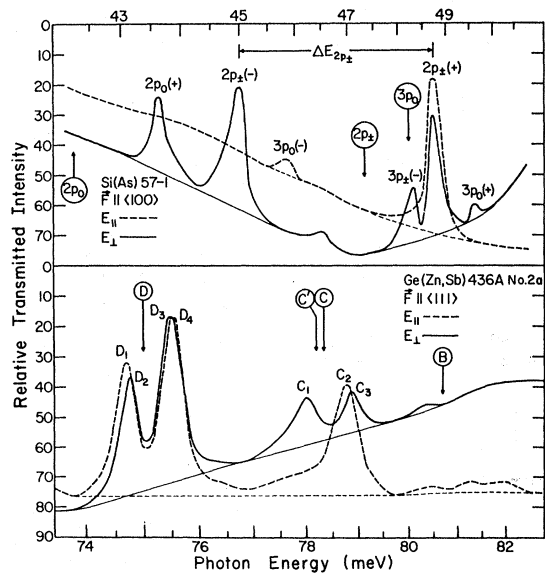


FIG. 17. Similar to Fig. 16 except that the $\langle 100 \rangle$ half sample of singly ionized zinc has been replaced by a $\langle 100 \rangle$ half sample of arsenic-doped silicon with a room-temperature resistivity of $\sim 6 \Omega \text{ cm}$. The arsenic spectrum was obtained with a grating blazed for 30μ with 30 grooves per mm.

15 to the data for the C components. In fitting C_4 , the point at $\sim 13 \times 10^8 \text{ dyn/cm}^2$ (see Fig. 14) was not included. If this point were included, this component would exhibit essentially no stress dependence. It is difficult to ascribe any components other than C_1 and C_4 to C' and even for these there is some doubt since neither has an intercept that is unambiguously equal in energy to C' . The observation of six components for the C line eliminates the possibility considered for $\vec{F} \parallel \langle 111 \rangle$ that the final

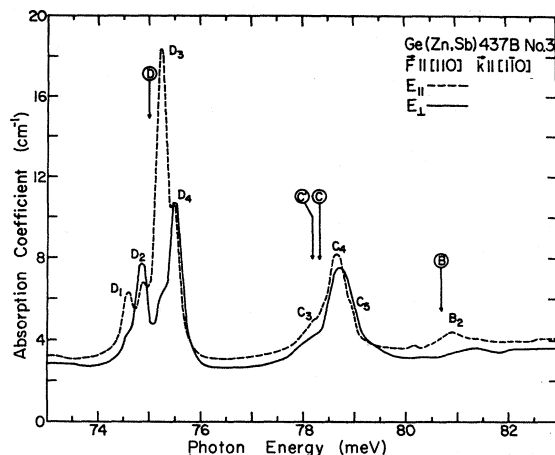


FIG. 18. Excitation spectrum of singly ionized zinc in germanium with a compressive force parallel to $[110]$ and light propagating along $[1\bar{1}0]$. The strain jig was used for this measurement. Liquid helium used as coolant.

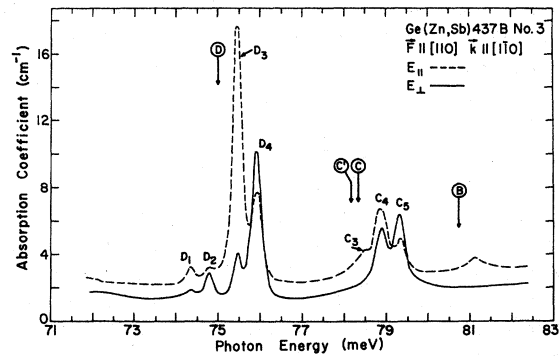


FIG. 19. Same as Fig. 18 except at a larger stress.

state for the C line is a Γ_7 level alone.

The inset to Fig. 10, the main spectrum of Fig. 10, and the spectrum of Fig. 14 demonstrate that the intensity of C_2 decreases with increasing stress while that of C_4 does not and, in fact, may increase. A comparison of C_5 with C_6 in Figs. 12 and 14, both stresses being somewhat inhomogeneous, demonstrates that the intensity of C_5 decreases relative to that of C_6 as the stress increases. These conclusions imply that C_2 and C_5 arise from the upper sublevel of the ground state, while C_4 and C_6 are from the lower sublevel. In addition, there is some evidence that C_3 persists even at the large strain of Fig. 14 and hence also arises from the lower sublevel of the ground state. From the linear fits to the C components it is found that the energy spacings of the pairs C_1 and C_3 , C_2 and C_5 , and C_4 and C_6 are, within experimental error, all equal to Δ'_{100} . However, in view of the energies and origins of the pairs of lines C_2 and C_5 and C_4 and C_6 , it follows that two pairs of excited sublevels must exist, each pair having an energy separation of $\sim \Delta'_{100}$. If it is assumed that C_1 , the component of lowest energy, has the upper sublevel of the ground state as initial state, then, taking into account the polarization properties of the components, the simplest interpretation of the C line is that its final state is the combination $\Gamma_7 + 2\Gamma_8$. Under stress, the two Γ_8 levels split by $\sim \Delta'_{100}$. This interpretation is compatible with the data for $\vec{F} \parallel \langle 111 \rangle$ provided that the two Γ_8 final states undergo virtually no splitting in that case. It is interesting to note that if the above interpretation of the C line is correct, then, for $\vec{F} \parallel \langle 111 \rangle$, the Γ_8 final state of the D line and the two Γ_8 final states of the C line behave in similar ways in that they exhibit virtually no splitting, while for $\vec{F} \parallel \langle 100 \rangle$ all three Γ_8 excited states again split in a similar way, although in this case the splitting is substantial, being $\sim \Delta'_{100}$.

3. Applied Force Along $\langle 110 \rangle$ Axis

The spectra obtained with $\vec{F} \parallel \langle 110 \rangle$ are shown in Figs. 18–20. Unlike the other two orientations

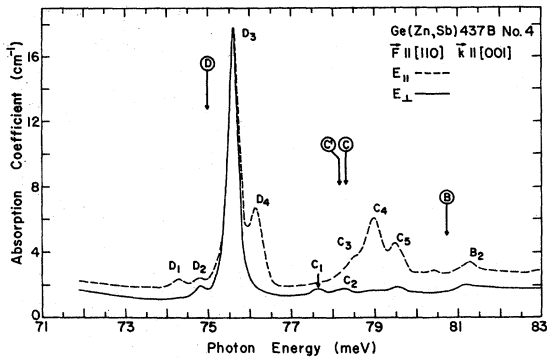


FIG. 20. Same as Figs. 18 and 19 but for light propagating along $[001]$, and, also, at a larger stress.

examined, the intensities of the stress-induced components for E_{\perp} depend upon the direction of light propagation \vec{k} . This may be seen by comparing the results in Figs. 18 and 19 with those in Fig. 20. In the first two cases, $\vec{F} \parallel [110]$ and $\vec{k} \parallel [1\bar{1}0]$, while the other result is for $\vec{k} \parallel [001]$. This effect has been discussed in I (see also Ref. 39). The decrease in intensity of the low-energy pair D_1 and D_2 as the stress is increased demonstrates that these two arise from the upper sub-level of the ground state. These data have been obtained with the strain jig and hence only the relative magnitudes of the stresses are known, having been gauged from the spacings of the D components. The energy spacings of D_1 and D_2 and D_3 and D_4 are the same and thus must be the splitting Δ'_{110} of the excited state (see I). The splittings of D_1 and D_3 and D_2 and D_4 are also the same and represent the ground-state splitting Δ'_{110} . Using Δ'_{110} as a gauge of the stress, the energies of the various components have been plotted and fitted to the straight lines shown in Fig. 21.

From Eq. (29) of I and the values given in Eqs. (1)–(4) it is predicted that $|\Delta'_{110}/\Delta^D_{110}| = 2.35 \pm 0.11$. From the plot of $|\Delta^D_{110}|$ as a function of $|\Delta'_{110}|$ given in Fig. 22, it is found that $|\Delta'_{110}/\Delta^D_{110}| = 2.50 \pm 0.06$, in good agreement with the value predicted. Even better agreement can be obtained if the slope of the straight line defining $\sim D_3$ in Fig. 15 were increased, the difference in slope between D_1 and D_4 being kept constant.

The shift in the center of gravity of the D components in Fig. 21 is found to be $(0.143 \pm 0.006) \times |\Delta'_{110}|$. By using Eq. (29) of I and the various results given above, the value of $a' - a_D$ listed in Table II is obtained. This value is in much better agreement with that obtained for $\vec{F} \parallel \langle 111 \rangle$ than that for $\vec{F} \parallel \langle 100 \rangle$. It is interesting to note that the numerical factor in the above shift is the same, within experimental error, as that given earlier for $\vec{F} \parallel \langle 111 \rangle$. This suggests that $\Delta'_{110} = \Delta'_{111}$ and

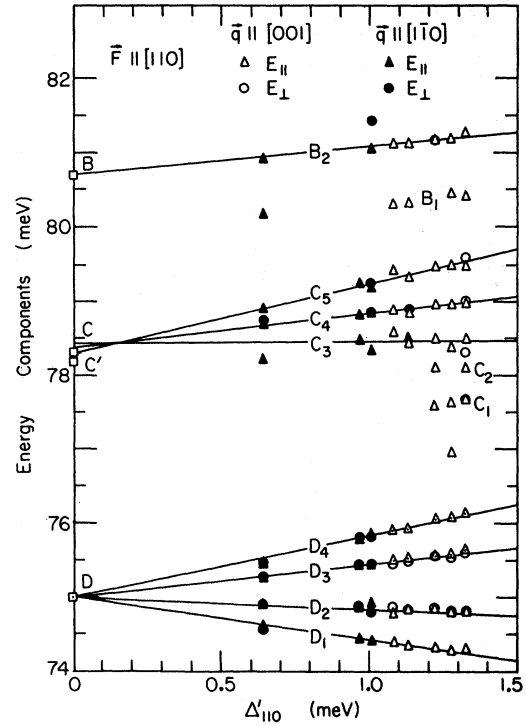


FIG. 21. Energies of the stress-induced components of the excitation spectrum of singly ionized zinc for $\vec{F} \parallel \langle 110 \rangle$ as a function of the ground-state splitting Δ'_{110} .

hence both are equal to Δ'_{100} , giving the isotropic case.¹ Such a stress isotropy has been observed for boron in silicon.⁴⁰ However, the results in Eqs. (1) and (3) do not support this and give $|\Delta'_{100}/\Delta'_{111}| = 0.87 \pm 0.04$. If the shifts obtained for $\vec{F} \parallel \langle 111 \rangle$ and $\vec{F} \parallel \langle 110 \rangle$, viz., $(0.150 \pm 0.006)|\Delta'_{111}|$ and $(0.143 \pm 0.006)|\Delta'_{110}|$, are equated, another determination of $|\Delta'_{100}/\Delta'_{111}|$ can be obtained using Eq. (29) of I. This ratio is found to be $1.17^{+0.30}_{-0.33}$, which, when the errors are taken into account, is in reasonable agreement with the value obtained directly.

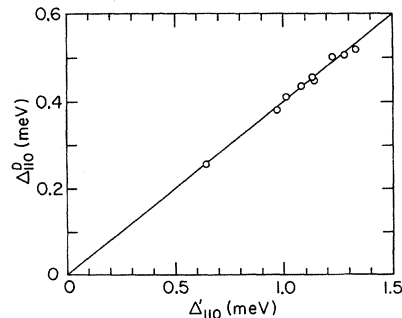


FIG. 22. Splitting of the excited state of the D line of singly ionized zinc as a function of the splitting of the ground state for $\vec{F} \parallel \langle 110 \rangle$.

In addition to predicting the splittings of the ground state and excited state of the D line, the parameters determined for $\vec{F} \parallel \langle 100 \rangle$ and $\vec{F} \parallel \langle 111 \rangle$ also should give the relative intensities of the D components. The signs of Δ'_{111} and Δ^D_{111} determine unambiguously the orderings of the sublevels of the two Γ_8 states of this transition. The energy eigenstates of the strain energy of an acceptor for $\vec{F} \parallel \langle 110 \rangle$ are Θ_μ ($\mu = -\frac{3}{2}, -\frac{1}{2}, \frac{1}{2}, \frac{3}{2}$) [given in Eq. (27) of I]. $\Theta_{\pm 3/2}$ are degenerate with an eigenvalue of $a'(s_{11} + 2s_{12})T - \frac{1}{4}(\Delta'^2_{100} + 3\Delta'^2_{111})^{1/2} \text{sgn}\Delta'_{111}$ and $\Theta_{\pm 1/2}$ belong to the eigenvalue $a'(s_{11} + 2s_{12})T + \frac{1}{4}(\Delta'^2_{100} + 3\Delta'^2_{111})^{1/2} \text{sgn}\Delta'_{111}$. Here $\text{sgn}\Delta'_{111}$ is $+1$ if Δ'_{111} is positive and -1 if it is negative. Similar results hold for the excited state. Note that there is an error in sign in these expressions as given in I. In the present case, Δ'_{111} is positive and thus the $\pm \frac{3}{2}$ sublevel of the ground state for $\vec{F} \parallel \langle 110 \rangle$ lies below the $\pm \frac{1}{2}$ sublevel. Since Δ^D_{111} is negative, the reverse ordering holds for the excited state. The intensities of the components depend upon the parameters u_D , v_D , γ , and δ (see Table XVIII of I⁴¹), where γ is given by Eq. (28) of I when $\Delta'_{111} > 0$, but, in general,

$$\gamma = x + (1 + x^2)^{1/2}, \quad (7)$$

where

$$x = (\Delta'_{100} / \sqrt{3} \Delta'_{111}). \quad (8)$$

The quantity δ is defined in the same manner, but for the excited state. We find that $\gamma = 1.62 \pm 0.03$ and $\delta = 13.6^{+2.7}_{-2.1}$, since x is positive for both states, corresponding closely to the parameters used to plot Figs. 6 and 7 of I. For a value of $v_D \approx \frac{1}{4}$ (see Sec. III B 2) and $T \approx 10^\circ \text{K}$, the predicted relative intensities are in satisfactory agreement with those observed for both directions of \vec{k} used in our experiments (see Figs. 18–20). For E_{\parallel} it is predicted that the relative intensities of the components are in the ratios $D_1^{\parallel} : D_2^{\parallel} : D_3^{\parallel} : D_4^{\parallel} : 0.33 : 0.20 : 0.31 : 0.16$, which become $0.07 : 0.04 : 0.25 : 0.13$ when the depopulation effect characteristic of $\Delta'_{110} = 1.3 \text{ meV}$ for Fig. 19 is included. For E_{\perp} and $\vec{k} \parallel [1\bar{1}0]$, it is found that $D_1^{\perp} : D_2^{\perp} : D_3^{\perp} : D_4^{\perp} : 0.09 : 0.52 : 0.16 : 0.22$, which for Fig. 19 reduces to $0.02 : 0.11 : 0.13 : 0.17$. As can be seen, these results are in good agreement with the experimental data. For the other two figures, Figs. 18 and 20, the predictions for E_{\parallel} are also well substantiated. For these two figures, Δ'_{110} is 0.64 and 1.32 meV , respectively. It is interesting to note that the component D_2^{\perp} , which is predicted to be the strongest of the transitions for E_{\perp} and $\vec{k} \parallel [1\bar{1}0]$, does indeed increase dramatically as the stress decreases. For E_{\perp} and $\vec{k} \parallel [001]$, it is predicted that $D_1^{\perp} : D_2^{\perp} : D_3^{\perp} : D_4^{\perp} : 0.06 : 0.31 : 0.55 : 0.08$, which, when the depopulation effects appropriate to Fig. 20 are taken into account, become $0.01 : 0.05 : 0.46 : 0.07$,

which is again in satisfactory agreement with the experiment. If in the above, the sign of Δ'_{100} is taken to be negative, then, since Δ^D_{100} has been shown by experiment to be of opposite sign to Δ'_{100} , both γ and δ are to be replaced by their reciprocals (see I) and v_D becomes negative. However, as pointed out in I, this does not affect the relative intensities predicted above.

The results for the C line for $\vec{F} \parallel \langle 110 \rangle$ show that there are three or more stress-induced components for this transition. This again rules out the possibility that this excitation is between a Γ_8 and Γ_7 state. We note that the energy spacings C_3 to C_4 and C_4 to C_5 are almost identical to each other and to Δ^D_{110} , as given by the spacings D_1 to D_2 and D_3 to D_4 . This suggests that the proposed two Γ_8 states of the C line for this direction of \vec{F} also split by the same amount as the Γ_8 final state of the D line. In the fits made to three of the C components in Fig. 21, no zero-stress components were used. It appears as though all three of these are due to splitting of the C line.

Nothing has been said, to this point, about the behavior of the B line under stress for any one of the three orientations. At most only two components have been observed for this line, as can be seen from Figs. 5, 15, and 21. In each case, a least-squares fit has been made to the well-behaved component using the zero-stress values of the line. For B_1 , in Figs. 15 and 21, the behavior appears to be nonlinear with stress and no fits have been made. However, it is clear that if a linear fit were made to either of these two lower-energy components, without any zero-stress values of B being included, the intercept obtained would be $\sim 80 \text{ meV}$, which is quite different from the zero-stress value of B . This result appears to predict the presence of a previously undetected excitation line between B and C .

IV. CONCLUSIONS

The experimental results show that the ordering of the levels of the ground state and the excited state of the D line are those given in Fig. 1 of I for uniaxial compression. In addition, for a uniaxial compression along a $\langle 110 \rangle$ direction, the ground state splits such that the $\Theta_{\pm 3/2}$ states are of lower energy than the $\Theta_{\pm 1/2}$ states, while the opposite is true for the excited state of the D line. These conclusions are unambiguous for the $\langle 111 \rangle$ and $\langle 110 \rangle$ directions but, for the $\langle 100 \rangle$ direction, the sign of b' has been chosen to be the same as that of the corresponding parameter for the valence band, as suggested by theory.³³ However, the relative ordering of the sublevels of the two Γ_8 states associated with the D transition has been determined without ambiguity.

We conclude that the C line is complex. The

simplest consistent interpretation is that this transition is to a $\Gamma_7 + 2\Gamma_8$ final state.

ACKNOWLEDGMENTS

Two of the authors take this opportunity to express their deep regret at the untimely death of their colleague, Fernando Barra. On his behalf,

they acknowledge the support he received from the University of Concepción, Chile, while this work was carried out. We also wish to thank A. K. Ramdas for useful discussions on the subject of this work and V. J. Tekippe and H. R. Chandrasekhar for assistance in use of the stress cryostat.

*Work supported in part by the National Science Foundation and the Advanced Research Projects Agency.

¹Deceased. Work carried out while on leave from the Instituto Central de Física, Universidad de Concepción, Concepción, Chile.

²S. Rodriguez, P. Fisher, and F. Barra, *Phys. Rev. B* **5**, 2219 (1972). This publication will be referred to as I. Note the following errata: Equation (7) in the present paper corrects Eq. (28) of I. The eigenvalues of $\Theta_{\pm(3/2)}$ and $\Theta_{\pm(1/2)}$ are interchanged. In Table XV of I, for $\Gamma_8 \rightarrow \Gamma_8$, the stress-induced component $\Gamma_6 \rightarrow \Gamma_7$ should have a transition probability of $2|D|^2$, not $2|D'|^2$ as given. However, the relative intensities are correct. In Table XVIII, for the transition $(1/2) \rightarrow (3/2)$ and E_1 for $k \parallel [001]$, the sign of the coefficient of u , should be changed.

³F. Barra and P. Fisher, *Phys. Lett. A* **27**, 711 (1968).

⁴F. Barra, P. Fisher, and S. Rodriguez, *Bull. Am. Phys. Soc.* **16**, 306 (1971).

⁵P. Fisher and H. Y. Fan, *Phys. Rev. Lett.* **5**, 195 (1960).

⁶R. D. Hancock and S. Edelman, *Rev. Sci. Instrum.* **27**, 1082 (1956); see also J. W. Edwards, *Semicond. Prod.* **6**, 30 (1963); *Semicond. Prod.* **6**, 34 (1963).

⁷E. K. Plyler, A. Danti, L. R. Blaine, and E. D. Tidwell, *J. Res. Natl. Bur. Stand. (U.S.) A* **64**, 29 (1960).

⁸L. R. Blaine, E. K. Plyler, and W. S. Benedict, *J. Res. Natl. Bur. Stand. (U.S.) A* **66**, 223 (1962).

⁹Manufactured by Charles M. Reeder and Co., Inc., 196 Victor Ave., Detroit 3, Mich.

¹⁰P. Fisher, W. H. Haak, E. J. Johnson, and A. K. Ramdas, in *Proceedings of the Eighth Symposium on the Art of Glassblowing* (American Scientific Glassblowing Society, Wilmington, Del., 1963), p. 136.

¹¹A. C. Rose-Innes, *Proc. Phys. Soc. Lond.* **72**, 514 (1958).

¹²R. L. Jones, Ph.D. thesis (Purdue University, 1968) (unpublished).

¹³V. J. Tekippe, H. R. Chandrasekhar, P. Fisher, and A. K. Ramdas, *Phys. Rev. B* **6**, 2348 (1972).

¹⁴G. R. Bird and M. Parrish, Jr., *J. Opt. Soc. Am.* **50**, 886 (1960).

¹⁵V. I. Sidorov, T. E. Sushko, and A. Ya. Shul'man, *Fiz. Tverd. Tela* **8**, 2022 (1966) [*Sov. Phys.-Solid State* **8**, 1608 (1967)].

¹⁶R. L. Jones and P. Fisher, *J. Phys. Chem. Solids* **26**, 1125 (1965).

¹⁷P. Fisher, R. L. Jones, A. Onton, and A. K. Ramdas, *J. Phys. Soc. Jap. Suppl.* **21**, 224 (1966).

¹⁸W. J. Moore, *Solid State Commun.* **3**, 385 (1965).

¹⁹R. L. Jones and P. Fisher (unpublished data).

²⁰H. Shenker, E. M. Swiggard, and W. J. Moore,

Tran. Met. Soc. AIME, **239**, 347 (1967).

²¹R. A. Chapman and W. G. Hutchinson, *Phys. Rev.* **157**, 615 (1967).

²²B. Pajot and Y. Darriot, *Phys. Lett.* **21**, 512 (1966).

²³K. S. Mendelson and H. M. James, *J. Phys. Chem. Solids* **25**, 729 (1964).

²⁴P. Fisher and A. K. Ramdas, in *Physics of the Solid State*, edited by S. Balakrishna, M. Krishnamurthi, and B. Ramachandra Rao (Academic, New York, 1969), p. 149.

²⁵J. Appel, *Phys. Rev.* **133**, A280 (1964).

²⁶R. L. Jones and P. Fisher, *Phys. Rev. B* **2**, 2016 (1970).

²⁷Performed by Battelle Memorial Institute, 505 King Avenue, Columbus, Ohio.

²⁸L. T. Ho and A. K. Ramdas, *Phys. Rev. B* **5**, 462 (1972).

²⁹Magnesium-doped germanium samples, obtained either from an ingot pulled from the melt or by diffusion, appear to be p type, L. T. Ho (private communication).

³⁰P. Fisher (unpublished data).

³¹Some features similar to these have been reported by D. C. Cronmeyer and W. N. Fetzner, *Bull. Am. Phys. Soc.* **6**, 426 (1961).

³²The pressure head used in the present measurements was not the same one whose calibration was given in Ref. 12. The present calibration was carried out using a tensile-stress apparatus (see Ref. 12).

³³J. H. Reuszer and P. Fisher, *Phys. Rev.* **135**, A1125 (1964).

³⁴G. L. Bir, E. I. Butikov, and G. E. Pikus, *J. Phys. Chem. Solids* **24**, 1467 (1963). Note that this reference was given incorrectly in I.

³⁵M. E. Fine, *J. Appl. Phys.* **26**, 862 (1955).

³⁶H. P. Soepangkat and P. Fisher (unpublished).

³⁷See, for example, N. C. Barford, *Experimental Measurements: Precision, Error and Truth* (Addison-Wesley, Reading, Mass., 1967), Chap. 3.

³⁸F. H. Pollak and M. Cardona, *Phys. Rev.* **172**, 816 (1968).

³⁹It should be noted that if the relative ordering of the sublevels of the two Γ_8 states in Fig. 1(b) of I is reversed, i.e., the signs of b' and b_D' changed, the sign of ν_D will also change.

⁴⁰R. L. Aggarwal and A. K. Ramdas, *Phys. Rev.* **137**, A602 (1965).

⁴¹H. R. Chandrasekhar, P. Fisher, A. K. Ramdas, and S. Rodriguez, *Phys. Lett. A* **41**, 137 (1972).

⁴²See correction to this table given in Ref. 1.